Preprint Cambridge Centre for Computational Chemical Engineering ISSN 1473 – 4273

Microkinetic Modeling of Fischer-Tropsch Synthesis over Cobalt Catalysts

Pooya Azadi [1], George Brownbridge [1], Immanuel Kemp [1], Sebastian Mosbach [1], John S. Dennis [1], Markus Kraft [1*]

released: 28 August 2014

[1] Department of Chemical Engineering
and Biotechnology
University of Cambridge
New Museums Site
Pembroke Street
Cambridge, CB2 3RA
United Kingdom
E-mail: mk306@cam.ac.uk

Preprint No. 145

Keywords: Fischer-Tropsch, cobalt catalyst, microkinetics, parameter estimation, activation energy

Edited by
Computational Modelling Group
Department of Chemical Engineering and Biotechnology
University of Cambridge
New Museums Site
Pembroke Street
Cambridge CB2 3RA
United Kingdom

Fax: + 44 (0)1223 334796
E-Mail: c4e@cam.ac.uk
World Wide Web: http://como.cheng.cam.ac.uk/

Abstract

We present a detailed microkinetic analysis of Fischer-Tropsch synthesis on a Co/γ-Al_2O_3 catalyst over the full range of syngas conversions. The experiments were performed in a Carberry batch reactor with initial H_2/CO ratios of between 1.8 and 2.9, temperatures of 469 and 484 K, and an initial pressure of 2 MPa. A reaction mechanism based on the hydrogen-assisted CO activation pathway, which comprises of 128 elementary reactions with 85 free parameters, was compiled to model the experimental results. Each of these elementary reactions belongs to one the following reaction groups: adsorption/desorption, monomer formation, chain growth, hydrogenation/hydrogen abstraction, or water-gas shift. A two-stage parameter estimation method, based on a quasi-random global search followed by a gradient-free local optimization, has been utilized to calculate the values of pre-exponential factors and activation energies. The use of data from batch experiments allowed for an effective analysis of dominating reactions at different stages of syngas conversion.

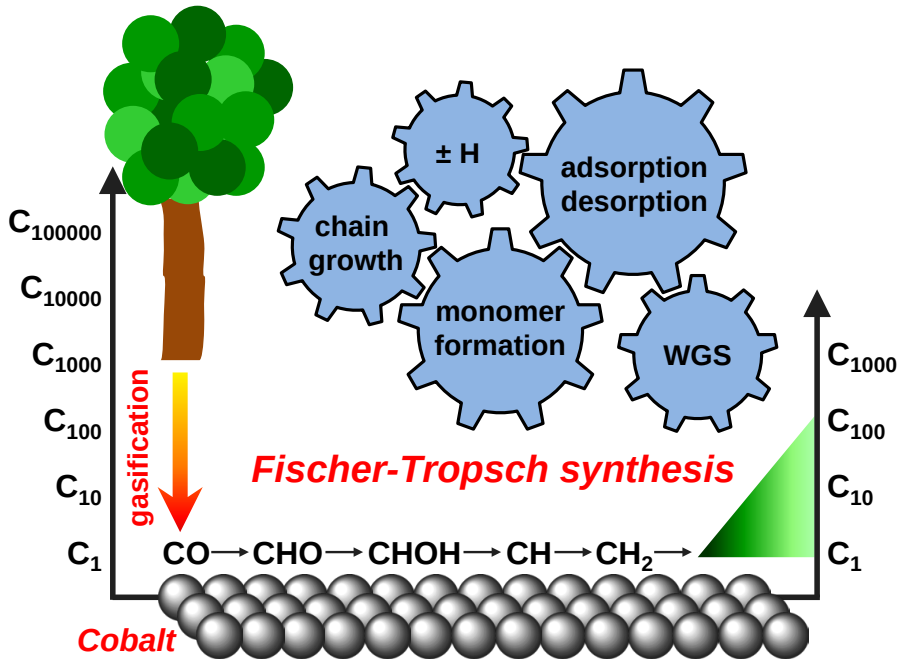

1 Introduction

The foreseeable decline in the supply of conventional oil [18] and the recent developments in the exploitation of unconventional gas and large-scale gasification technologies have together resulted in a renewed interest in Fischer-Tropsch (FT) synthesis. In this process, mixtures of CO and H_2 are catalytically converted into complex mixtures of hydrocarbons via successive deoxygenation and hydrogenation of carbon monoxide, followed by addition of the resultant CH_x monomers to growing hydrocarbon chains. Despite the apparent simplicity of the chemistry, fundamental aspects of the surface reactions in FT synthesis, such as the dominant CO activation pathway, have been highly controversial subjects within the field of heterogeneous catalysis for several decades [7, 8, 12, 19, 21].

Due to the large number of reacting species, readsorption and conversion of primary products, difficulties in measuring surface intermediates, and coverage-dependent reaction rates detailed mechanistic modeling of the FT synthesis is highly complex. Furthermore, even when considering the smallest number of elementary reactions sufficient to account for the major FT products, there remains more than one set of reaction rate constants, corresponding to different fractional surface coverages, from which the behavior of the system can be predicted. In other words, as any serviceable FT mechanism involves upwards of 40 free parameters (i.e. pre-exponential factors and activation energies), the system can remain underdetermined even when a large number of experimental data points are available. The use of systematic and semi-automated methods for parameter estimation, as opposed to just manually adjusting parameter values, make it easier to detect and understand potentially underdetermined parameters. One can see [14, 25] as examples of recent efforts towards modeling of the FT synthesis reactions.

Herein, we present a detailed microkinetic analysis of the Fischer-Tropsch reactions on a Co/γ-Al_2O_3 catalyst over the full range of syngas conversion. A two-stage parameter estimation method, based on a quasi-random global search followed by a local optimization [4, 16, 17], has been utilized to systematically calculate suitable values of pre-exponential factors and activation energies. A reaction mechanism based on the hydrogen-assisted CO activation pathway [7, 8, 12, 19], comprising of 128 elementary reactions with a total of 85 free parameters, was implemented to simulate 1176 measured data points across 8 experiments. The experiments were carried out in a batch reactor at H_2/CO ratios between 1.8 and 2.9, temperatures of 469 and 484 K, and initial pressures of approximately 2 MPa. The experiments were run to completion, which meant that several different reactions were dominant at different stages of the process. At low conversions the primary reactions (e.g. monomer formation and chain growth) dominated, however, as the process progressed the secondary reactions (e.g. alkene readsorption and water-gas shift) became more important.

The agreement between experiment and model was quantified using a least-squares objective function, which is explained in the Computational Methods section. The initial values of the activation energies and pre-exponential factors were chosen from previous studies based on Density Functional Theory (DFT) and transition state theory, respectively. However, due to the oversimplified nature of these first-principle methods, particularly in consideration of surface composition, the findings of such studies are often associated with large uncertainties and they are only able to provide limited insight into the kinetics of

FT synthesis (see Supporting Information). Hence, the search for optimum value of each parameter was conducted within reasonable bounds around its initial value determined by relevant first-principle calculations.

2 Experimental Section

2.1 FT synthesis

The FT experiments were carried out using a Carberry spinning basket batch reactor (Autoclave Engineers, USA) as shown in Figure 1 with a free volume of 296 ml. The rotational speed of the basket was set at approximately 260 rpm. After loading the catalyst, the reactor was purged with nitrogen, evacuated and heated to the reaction temperature using electrical band heaters. Then, the reactor was charged to the desired pressure with syngas. The reactor pressure was measured using a pressure gauge (Swagelok, USA) with a 2.5 MPa range and a precision of $\pm$ 0.02 MPa. The initial compositions and reactor pressures for each experiment are given in Table 1. Gas samples were taken from the reactor during the course of each experiment and analyzed using a gas chromatograph (Agilent 7890A, USA) equipped with TCD and FID to determine the composition of the reactor contents. Argon was used as an internal standard to calculate the partial pressure of each compound from the GC results. Selected experiments were repeated to ensure the reproducibility of the results.

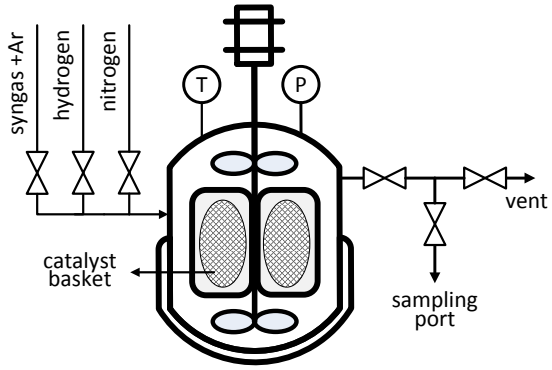

Figure 1: *Schematic diagram of Carberry spinning basket reactor.*

2.2 Catalyst preparation and characterization

The experiments were carried out using a 12 wt% Co/γ-Al_2O_3 catalyst at a loading of 4.3 – 5.0 g. The catalyst was prepared by impregnation of the support with a cobalt nitrate precursor (Sigma-Aldrich, UK) using an incipient wetness method. Following impregnation, the catalyst was dried at 363 K and calcined at 673 K for 4 h in flowing air (200 ml/min STP). The catalyst was then reduced in flowing hydrogen (200 ml/min STP) at 673 K for 4 h, and finally passivated at room temperature by exposing the catalyst to

Table 1: *Initial process conditions for the Cobalt experiments.*

Exp.	T K	P_{total} MPa	P_{CO} MPa	P_{H_2} MPa	P_{Ar} MPa	m_{cat} g
1	469	1.90	0.65	1.19	0.06	5.0
2	469	2.10	0.64	1.39	0.07	5.0
3	469	2.10	0.58	1.44	0.08	5.0
4	469	2.08	0.52	1.48	0.08	4.3
5	484	1.97	0.50	1.39	0.08	5.0
6	484	2.01	0.57	1.37	0.07	5.0
7	484	2.01	0.61	1.33	0.07	5.0
8	484	1.99	0.49	1.42	0.07	5.0

an gas mixture of 2% oxygen in nitrogen, progressively increasing the oxygen content to 10% over the course of 4 h. The passivated catalyst was reduced in H_2 again in situ prior to the experiments. X-ray diffraction patterns (Figure 2) were collected for 2θ from 20° to 80° using a Philips X'Pert Diffractometer at a rate of 0.0015° s^{-1}. The Scherrer equation was used to calculate the metal dispersion from the XRD spectrum. The BET surface area, support pore volume and average pore diameter were obtained for one sample of the catalyst using a Micromeritics catalyst characterization system (TriStar 3000, USA). The characteristics of that catalyst sample are summarized in Table 2.

Table 2: *Characteristics of the catalyst used in the FT experiments and microkinetic analysis.*

Parameter	Value	Unit
BET surface area	129	m^2/g
Pore volume	0.55	cm^3/g
Pore diameter	12.2	nm
Pellet diameter	3.0	mm
Co loading	12.0	wt%
Dispersion	11.1	%

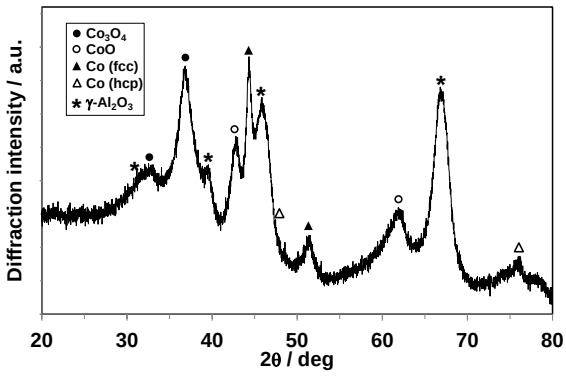

Figure 2: *XRD pattern of Co/γ-Al_2O_3 catalyst after multiple batch runs and exposure to air.*

3 Computational Methods

3.1 Parameter estimation

A total of 128 elementary reactions, listed in Table 4, with 85 free parameters were considered in this microkinetic study. The analysis was made more difficult by the lack of information about the concentrations of the species on the surface of the catalyst and disagreement among the activation energies reported in DFT studies (see Table S.2). Partially due to these complexities, the parameter estimation was carried out iteratively. At each iteration the scope of the optimization was increased, focusing on improving the fit of the model to the partial pressures of a wider range of species. As part of this strategy, the bounds on the parameters were often adjusted based on the results of previous iterations. When it was considered appropriate, new reactions were also added to the mechanism, for example, the water-gas shift reactions (22–24) were only added after most of the other reactions had been adjusted satisfactorily. Despite focusing on subsets of the parameters, particularly during the early stages, all of the parameters were included in the optimization at each iteration due to the high level of interconnectivity between each part of the model and the concentrations of the measured species.

At each iteration, parameter estimation was performed using a two-stage algorithm [4, 17]. The first stage was a global search, over the region defined by the parameters' bounds, conducted using low discrepancy points generated using a Sobol [22] sequence. The second stage took the best points found in the global search and refined the parameter values using a local valley-descending optimization routine. Initially the Levenberg-Marquardt gradient-based algorithm [15] was used for the local optimization although for later iterations the gradient-free Hooke and Jeeves' algorithm [10] was used instead as it was found to perform better. The best set of values found at this stage were then used to inform the next iteration.

A Sobol sequence was chosen to generate the points as they are guaranteed to be more uniformly distributed, in a strict mathematical sense, than (pseudo-)randomly generated points. With this number of parameters the Sobol sequence is also a more efficient sampling method than a full factorial design, which would require 2^{85} points as it includes

every combination in which the value of each parameter was set either high or low. Compared to this, only a relatively small number of points ~50–2000 were evaluated at each iteration and yet the inclusion of this step still greatly improved the quality of the optima found during the subsequent local optimization by allowing the optimization to escape the local minima containing the initial point of each iteration. This is particularly important given that the objective function surfaces associated with chemical kinetic systems are known to have a large number of local minima making the probability of finding the global one using only local optimization algorithms very small.

During both stages the agreement between experimental and model responses was quantified using the weighted least-squares objective function,

$$\Phi = \sum_{i}^{N_{\text{species}}} \sum_{j}^{N_{\text{samples}}} \left(\frac{P_{ij}^{\text{exp}} - P_{ij}^{\text{model}}}{\sigma_{ij}} \right)^2 , \tag{1}$$

where P_{ij}^{exp} is the experimentally measured partial pressure, P_{ij}^{model} is the corresponding model response, and σ_{ij} is used to weight the contribution of specie i in sample j. Weighting is required to allow the meaningful comparison of responses that take values that differ from each other by orders of magnitude [4, 17]. The value of σ for each data point was calculated systematically based on the level of uncertainty in the values measured in the experiments. The exact relation used was $\sigma_{ij} = a_i \, P_{ij}^{\text{exp}} + b_i$, which accounts for both the relative precision of the measuring devices through a and their measurement resolutions through b. The values used for a and b are given in Table 3.

Table 3: *Coefficients used for calculating the weight terms, σ_{ij} in the objective function.*

	CO	H_2	CO_2	CH_4	C_2H_6	C_3H_8	C_4H_{10}	C_5H_{12}	C_2H_4	C_3H_6	C_4H_8	C_5H_{10}
a %	3	20	1	0.5	1	1	1	1	1	0.5	0.5	1
b (Pa)	1000	10000	300	600	30	50	50	40	10	20	10	5

4 Results and Discussion

The key assumptions behind the presented kinetic model can be summarized as follow: i) the reactor is isothermal and homogeneous, ii) the rate of reaction is controlled by intrinsic surface kinetics and not mass transfer, iii) the catalyst only contains one type of active site and all reactions occur in a competitive manner on the surface of metal nanoparticles, iv) the pre-exponential factors and activation energies are coverage-independent, and v) the yields of oxygenated hydrocarbons throughout the reaction are negligible.

A schematic diagram of the essential pathways in FT synthesis, represented by simplified reaction groups and typical links among them, is shown in Figure 3. In order to minimize the number of parameters in the model, parallel pathways within each reaction group (i.e. each box in Figure 3) were avoided. For example, concerning the monomer formation group, only elementary reactions representing hydrogen-assisted CO deoxygenation

were considered and the carbide mechanism was excluded from the analysis. Likewise, the addition of carbene (CH_2) to C_nH_{2n+1} for $n \geqslant 2$ was assumed to be the sole pathway responsible for hydrocarbon chain growth, although it is possible that the addition of other types of CH_x monomers to C_nH_y growing species also have a considerable contribution. Therefore, the rate of conversion between any two species within each group in the present model, essentially, represents the overall conversion rate resulting from all possible pathways among them.

The absence of parallel pathways within each reaction group, however, does not rule out the presence of parallel pathways for the consumption (or generation) of gas species. For instance, one can see from Figure 3 that several pathways for the consumption (and generation) of hydrogen gas exist in the model. As an example, a C_nH_{2n+2} molecule can be generated via hydrogenation of a C_nH_{2n+1} growing chain, or via readsorption and subsequent hydrogenation of a previously desorbed C_nH_{2n} molecule.

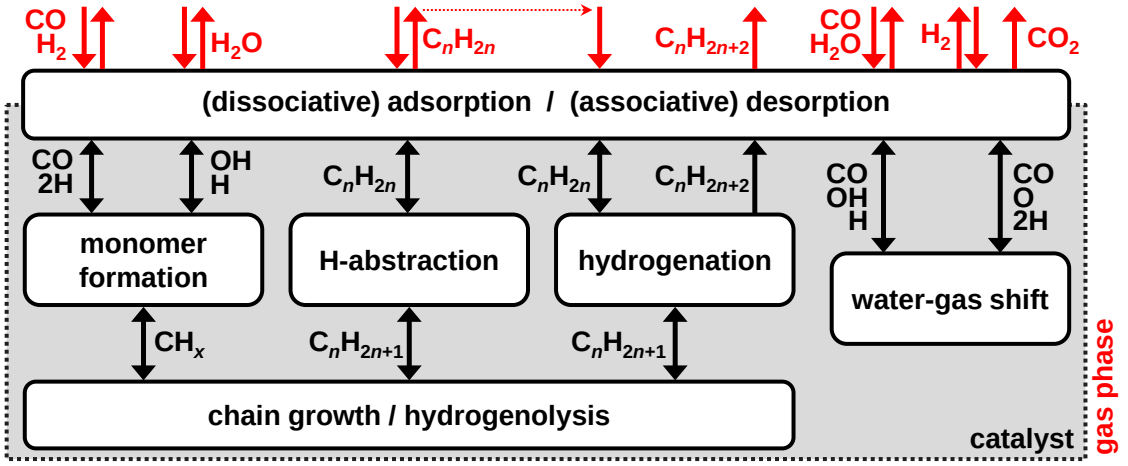

Figure 3: *Flow diagram for the reaction mechanism.*

The elementary reaction steps included in the presented microkinetic model, along with their respective pre-exponential factors and activation energies, are given in Table 4. The experimental results and model responses for single carbon compounds, paraffins, and olefins are plotted in Figures 4, 5, and 6, respectively. In line with the findings of previous DFT and isotope studies [19, 20], the adsorption of hydrogen and CO (reactions 1 & 2), and the first CO hydrogenation step (reaction 33) are found to be equilibrated throughout each experiment.

In order to account for the dependence of the rates of alkene adsorption/desorption (reactions 5 – 31) and alkyl growth (reactions 40 – 65) on the number of carbon atoms the equation

$$A_{C_n} = A_{C_4}\left[1 + c\left(1 - 1/(n-2)\right)\right],\ 4 \leqslant n \leqslant 30, \tag{2}$$

has been utilized to calculate the values of the pre-exponential factors of these reactions as a function of carbon number, n, and the value of the pre-exponential for the relevant reaction involving the C_4 specie, A_{C_4}. For each type of reaction (i.e. adsorption, desorption, and growth) a separate value of c was used and each was treated as a free parameter in the model.

As shown in Figure 4, the model responses for the C_1 compounds are in a close agreement with the experimental data. The model is reasonably able to predict the evolution of paraffins and olefins, see Figures 5 and 6. Importantly, the rapid decline in the yields of the olefins due to readsorption and subsequent conversion at high CO conversions is captured well by the current model.

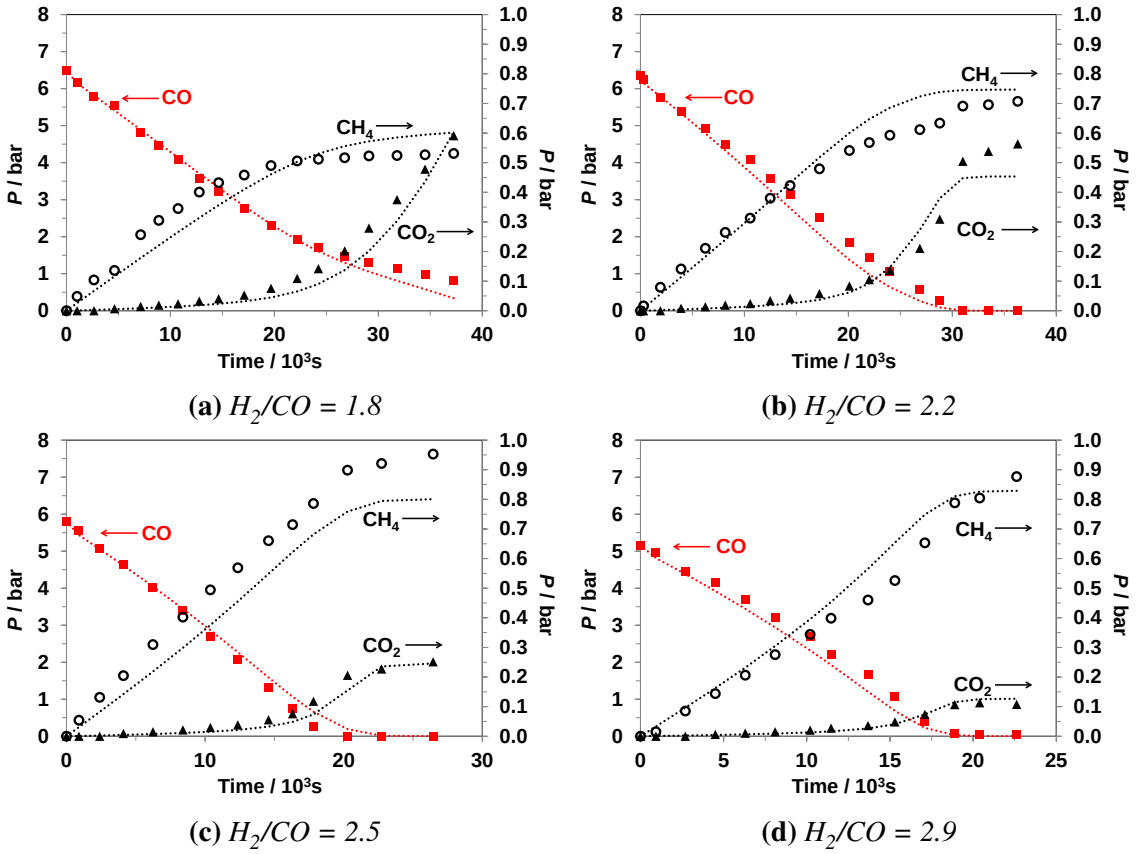

(a) $H_2/CO = 1.8$ **(b)** $H_2/CO = 2.2$

(c) $H_2/CO = 2.5$ **(d)** $H_2/CO = 2.9$

Figure 4: *The partial pressures of C_1 species at 469 K and different H_2/CO ratios.*

The fractional surface coverage profiles obtained from the model, for various initial compositions, are plotted as functions of syngas conversion in Figure 7. Based on the simulation results, the fractional concentrations on the catalyst surface decrease in the following order: CO > OH > H > free sites > C_nH_{2n+1} > CH_x > C_nH_{2n} > O. The fractional surface coverages of O (not shown in the figures) were considerably lower than those of the other groups. There are uncertainties associated with the number of sites each surface specie attaches to, which then affects the number of free sites consumed or produced in the relevant reactions. Considering the range over which the fractional concentration of free sites varies throughout the simulations, the addition or elimination of one free site from a reaction would be equivalent to a change in the activation energy of that reaction of up to 10 kJ/mol.

The value obtained from the parameter estimation for the heat of adsorption of hydrogen on cobalt is in agreement with calorimetric studies [9], which also indicated that the differential heat of adsorption of hydrogen on cobalt is almost independent of the hydrogen surface coverage. In contrast, the differential heat of adsorption of CO on cobalt dra-

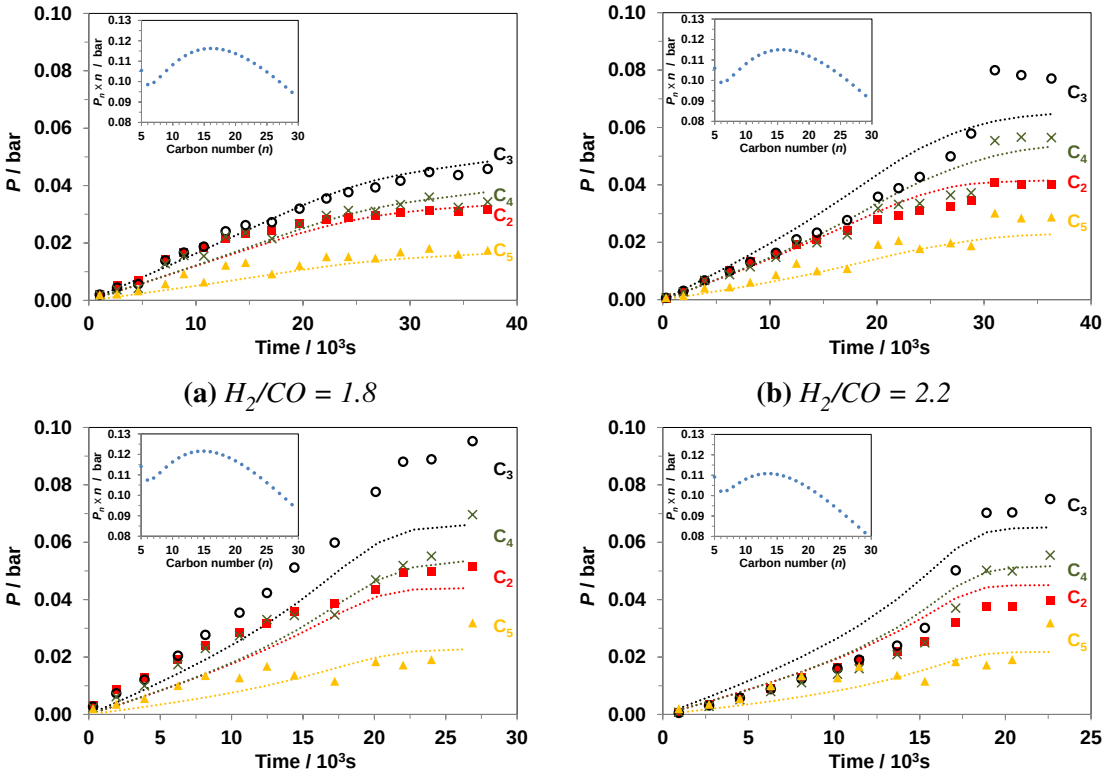

(a) $H_2/CO = 1.8$ **(b)** $H_2/CO = 2.2$

(c) $H_2/CO = 2.5$ **(d)** $H_2/CO = 2.9$

Figure 5: *The partial pressures of paraffins at 469 K and different H_2/CO ratios. The inserts show the weight distribution ($P_n \times n$) of higher hydrocarbons corresponding to the last point in each simulation.*

matically decreases with increasing CO surface coverage [9, 19]. This phenomenon is primarily attributed to the difference in the electronic structures of different types of catalytic sites (e.g. planar, edge, corner, terrace, etc.). One can expect that the reactivity of an adsorbed CO molecule is strongly influenced by the atomic coordination number of the catalytic site on which it is adsorbed. However, due to lack of quantitative information and to avoid further complexities, the coverage-dependency of the heat of adsorption and the subsequent reactions of the adsorbed molecules of carbon monoxide were not considered in this study.

The size of the active material nanoparticles and the identity of the catalyst support are among the factors that can, in principle, dramatically alter the activity of a given metal catalyst. Nevertheless, several studies have shown that the activity of cobalt catalysts for FT synthesis is independent of the crystallite sizes for nanoparticle sizes greater than about 6 – 8 nm [1–3, 11], which corresponds to metal dispersions of up to 12% – 16%. As the metal dispersion of a typical cobalt catalysts, including the catalyst utilized in the present study, is usually below these values the cobalt-catalyzed FT reactions are often regarded to be size-insensitive. It was also shown that, within a typical range of metal dispersion (e.g. 2% – 12%), the nature of the support material has an insignificant effect on the turnover frequencies observed on cobalt catalysts during FT synthesis [11]. The above evidence from literature, in support of the structure-insensitivity of cobalt-catalyzed FT synthesis,

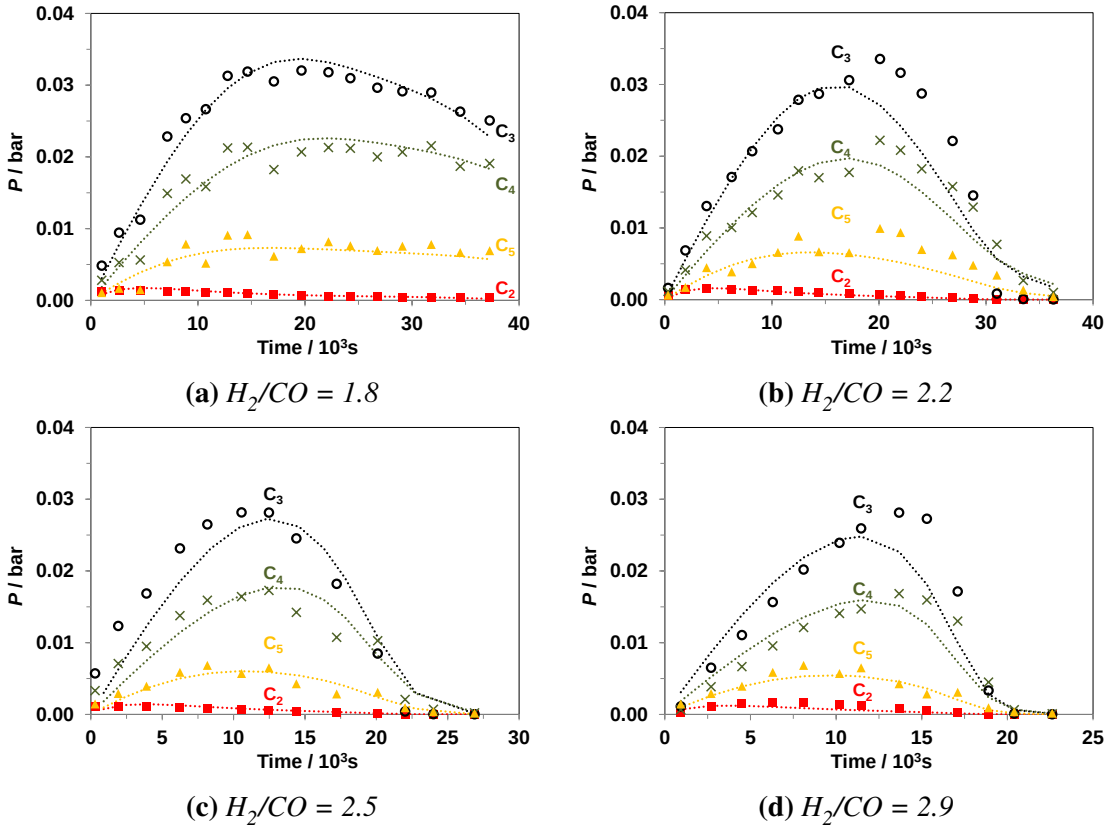

(a) $H_2/CO = 1.8$ **(b)** $H_2/CO = 2.2$

(c) $H_2/CO = 2.5$ **(d)** $H_2/CO = 2.9$

Figure 6: *The partial pressures of olefins at 469 K and different H_2/CO ratios.*

suggests that the present analysis could, to a reasonable extent, be applicable to a wide range of cobalt-catalyzed FT systems.

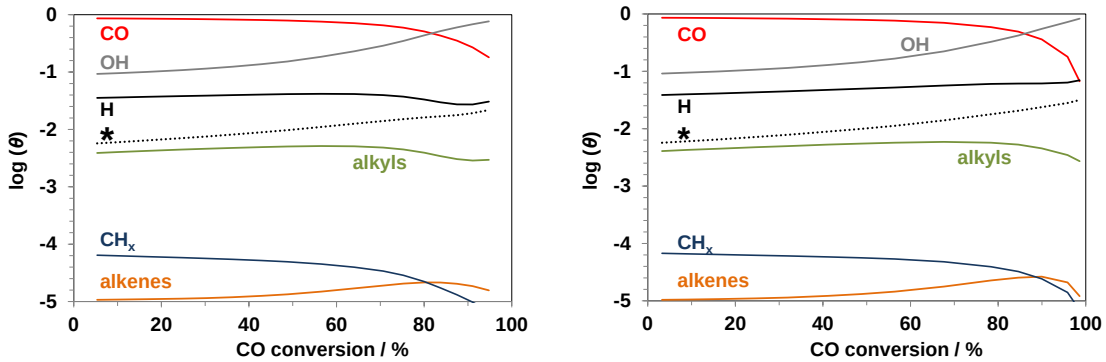

(a) $H_2/CO = 1.8$ **(b)** $H_2/CO = 2.2$

(c) $H_2/CO = 2.5$ **(d)** $H_2/CO = 2.9$

Figure 7: *Fractional surface coverage against CO conversion at 469 K and different initial H_2/CO ratios.*

Table 4: *List of elementary reactions and their pre-exponential factors and activation energies obtained from parameter estimation. The units of the activation energies (E_f and E_r) and the pre-exponential factors (A_f and A_r) are kJ mol^{-1} and Pa^{-n} s^{-1} respectively where n is unity for A_f of adsorption reactions and zero for all other reactions.*

Elementary step		A_f	E_f	A_r	E_r
Adsorption / Desorption					
1	$H_2 + 2* \rightleftharpoons 2H*$	1.0×10^3	-	6.8×10^{12}	48.1
2	$CO + * \rightleftharpoons CO*$	1.0×10^3	-	1.9×10^{16}	86.7
3	$C_2H_4 + 2* \rightleftharpoons C_2H_4**$	1.3×10^7	32.2	1.0×10^{17}	154.8
4	$C_3H_6 + 2* \rightleftharpoons C_3H_6**$	5.4×10^{10}	71.9	4.1×10^{13}	91.9
5 – 31	$C_nH_{2n} + 2* \rightleftharpoons C_nH_{2n}**$	3.7×10^{17} [a]	133.6	1.9×10^{13} [b]	90.4
32	$H_2O + 2* \rightleftharpoons OH* + H*$	6.0×10^8	58.9	1.8×10^{13}	122.8
Monomer formation					
33	$CO* + H* \rightleftharpoons HCO* + *$	8.4×10^{12}	128.1	1.9×10^{12}	54.1
34	$HCO* + H* \rightleftharpoons HCOH**$	6.1×10^{15}	84.3	8.1×10^8	121.8
35	$HCOH** + 2* \rightleftharpoons CH*** + OH*$	2.2×10^{13}	44.0	5.5×10^{10}	75.1
36	$CH*** + H* \rightleftharpoons CH_2** + 2*$	1.0×10^{13}	34.7	4.2×10^{10}	18.8
Chain growth					
37	$CH_2** + CH_2** \rightleftharpoons C_2H_4** + 2*$	1.2×10^{14}	4.5	5.6×10^5	28.5
38	$C_2H_5* + CH_2** \rightleftharpoons C_3H_7* + 2*$	3.0×10^{12}	39.5	1.5×10^{13}	107.2
39	$C_3H_7* + CH_2** \rightleftharpoons C_4H_9* + 2*$	1.6×10^{14}	57.3	4.9×10^6	57.8
40 – 65	$C_nH_{2n+1}* + CH_2** \rightleftharpoons C_{n+1}H_{2n+3}* + 2*$	5.0×10^{13} [c]	53.1	6.8×10^{11}	163.3
Hydrogenation / H-abstraction					
66	$CH_2** + H* \rightleftharpoons CH_3* + 2*$	1.5×10^{14}	69.6	4.7×10^9	52.9
67	$C_2H_4** + H* \rightleftharpoons C_2H_5* + 2*$	6.8×10^{16}	126.6	2.8×10^7	34.1
68	$C_3H_6** + H* \rightleftharpoons C_3H_7* + 2*$	1.5×10^{13}	59.2	4.1×10^{10}	53.3
69 – 95	$C_nH_{2n}** + H* \rightleftharpoons C_nH_{2n+1}* + 2*$	1.1×10^{14}	66.8	1.9×10^{12}	68.2
96	$CH_3* + H* \rightarrow CH_4 + 2*$	3.4×10^{17}	141.0		
97	$C_2H_5* + H* \rightarrow C_2H_6 + 2*$	1.5×10^{14}	131.0		
98 – 125	$C_nH_{2n+1}* + H* \rightarrow C_nH_{2n+2} + 2*$	1.1×10^{15}	138.8		
Water-gas shift					
126	$OH* + OH* \rightarrow H_2O + O**$	9.3×10^{11}	135.3		
127	$CO* + O** \rightarrow CO_2 + 3*$	8.7×10^8	18.2		
128	$H* + O** \rightarrow OH* + 2*$	2.2×10^{16}	86.2		

[a] A_{f,C_4} in Equation 2 with $c = 1.83$.
[b] A_{r,C_4} in Equation 2 with $c = 0.73$.
[c] A_{f,C_4} in Equation 2 with $c = 2.29$.

5 Conclusions

In summary, a detailed microkinetic model of Fischer-Tropsch synthesis on a Co/γ-Al_2O_3 catalyst has been developed. The model is capable of predicting FT product distributions (i.e. paraffins, olefins, and carbon dioxide) over the full range of syngas conversions for initial H_2/CO ratios of between 1.8 and 2.9 and temperatures of 469 and 484 K. The model presented here can serve as a starting point for future studies targeting subsets of the elementary reactions to fine tune their rate parameters, or for microkinetic studies conducted with different catalysts.

6 Acknowledgements

This work was partially supported by the E3C3 project (no. 4274), which was selected by the European INTERREG IV A France (Channel) - England Cross-border Cooperation Programme, and is co-financed by the European Regional Development Fund (ERDF). Markus Kraft also acknowledges support from the Singapore National Research Foundation under its Campus for Research Excellence And Technological Enterprise (CREATE) program.

7 Supporting information

7.1 Mass transfer considerations

No noticeable change in the rate of reaction occurred when the rotational speed of the catalyst basket was changed, suggesting that the reaction was not limited by external mass transfer but instead by the intrinsic surface kinetics. Further evidence supporting this assumption is that the apparent activation energy calculated from the results shown in Figure S.1, which shows the effect of temperature on the initial turnover frequency of CO consumption, is approximately equal to 121 kJ/mols. We note that a much weaker dependency on the temperature would have been observed if the reactions were limited by intra-particle mass transfer. This value is also consistent with the values reported in previous studies on cobalt-catalyzed FT syntheses (see Table S.1).

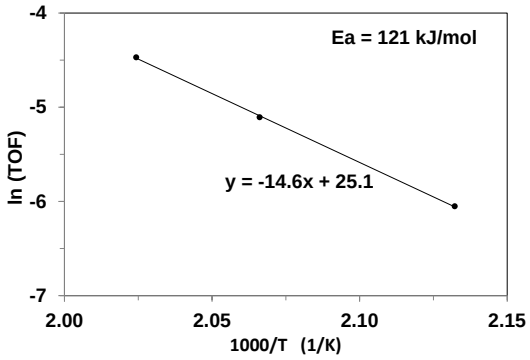

Figure S.1: *Effect of temperature on CO turnover frequency. The slope of the fitted line is equal to E/R where E is the apparent activation energy and R is the gas constant.*

Table S.1: *Selected turnover frequencies (TOF) and C_{5+} selectivity of cobalt-catalyzed FT synthesis found in the literature.*

Support	T K	P MPa	H_2/CO	Particle size nm	Conv. %	TOF $10^{-3}s^{-1}$	C_{5+} wt%	Ref.
SiO_2	473	2	2		8 – 49	7 – 18	86 – 92	[13]
CNF	483	3.5	2	2.6 – 16	~60	1.4 – 23	76 – 85	[1]
γ-Al_2O_3	483	2	2.1	5 – 15		31 – 63	77 – 84	[2]
γ-Al_2O_3	473 – 503	0.18	10		4.3	3 – 10		[24]
γ-Al_2O_3	493	0.18	5 – 15			3 – 9		[24]

7.2 Carbon balance

Figure S.2 shows the selectivity of the C_{5+} hydrocarbons as the CO is converted in the experiments. As can be seen from this figure, the C_{5+} selectivity is between 65% and 78%, which is in line with the observations of the studies listed in Table S.1. It is worth mentioning that within the conversion range shown here, the amount of carbon on the surface of the catalyst constitutes less than 2% of the total carbon in the reactor and so is negligible in comparison to the quantity of C_{5+} hydrocarbons.

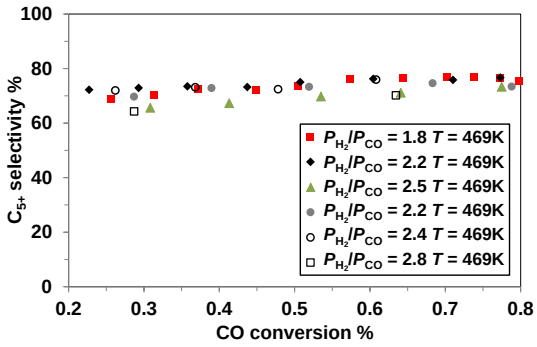

Figure S.2: *Variation of C_{5+} selectivity with CO conversion at different temperatures and initial syngas compositions.*

7.3 Initial catalyst deactivation and reproducibility of results

It is generally observed that the activity of each fresh batch of catalyst declines over an initial period of use before stabilizing. The results presented in this study were collected after eight initial batch runs, which was found to be an adequate period of use to avoid variation in performance during subsequent runs. In addition, some of the experiments were repeated to check that the catalyst activity stayed stable during the course of the experiments used for the analysis. As shown in Figure S.3, the differences between the replicated runs were within a few percent.

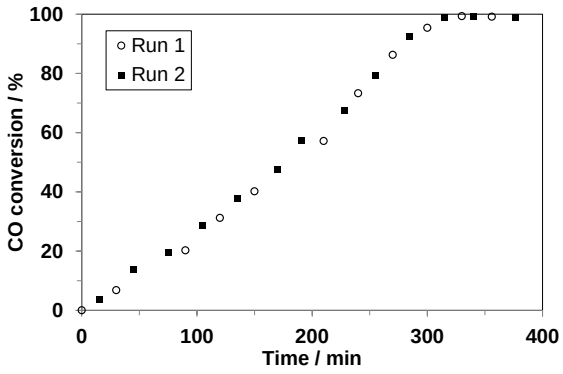

Figure S.3: *Reproducibility of results represented by CO conversion during two experimental runs performed under the same conditions.*

7.4 Selected values of activation energy from previous DFT studies

Table S.2: *Selected values of the forward and reverse activation energies (E_f/E_r), in kJ mol^{-1}, based on DFT calculations in the literature.*

Elementary step	ref [19]	ref [12]	ref [23]	ref [6]	ref [5]
$H_2 + 2* \rightleftharpoons 2H*$	50 / 65		14 / 85		
$CO + * \rightleftharpoons CO*$			0 / 112		
$CO* + * \rightleftharpoons C* + O*$	376 / 115	272 / 70	153 / 129		
$C* + H* \rightleftharpoons CH* + *$	40 / 213		161 / 23	80 / 118	
$CO* + H* \rightleftharpoons HCO* + *$	138 / 38	126 / 96	101 / 0		126 / 11
$HCO* \rightleftharpoons CH* + O*$	92 / 82	96 / 76			
$HCO* + H* \rightleftharpoons HCOH* + *$	90 / 161				119 / 81
$HCOH* + * \rightleftharpoons CH* + OH*$	106 / 89				
$CH* + H* \rightleftharpoons CH_2* + *$	36 / 40		60 / 102	63 / 28	
$OH* + H* \rightleftharpoons H_2O + 2*$	62 / 205				
$O* + H* \rightleftharpoons OH* + *$	47 / 151		108 / 57		
$HCO* + H* \rightleftharpoons CH_2O* + *$	14 / 147	43 / 34			53 / 36
$CH_2O* + * \rightleftharpoons CH_2* + O*$	157 / 78	82 / 67	108 / 85		92 / 133
$CH_2* + CH_2* \rightleftharpoons C_2H_4**$			10 / 149	68 /	
$C_2H_4** + H* \rightleftharpoons C_2H_5 + 2*$			3 / 42		
$C_2H_4** \rightleftharpoons C_2H_4 + 2*$			55 / 0		
$CH_2* + H* \rightleftharpoons CH_3* + *$			34 / 106	58 / 71	
$CH_3* + H* \rightleftharpoons CH_4 + 2*$			11 / 14	93 /	
$CH_2O* + H* \rightleftharpoons CH_3O*$					83 / 98
$CH_3O* + H* \rightleftharpoons CH_3OH*$					140 / 77
$CO* + H* \rightleftharpoons COH*$					174 / 92
$COH* + H* \rightleftharpoons CHOH*$					82 / 10
$CHOH* + H* \rightleftharpoons CH_2OH*$					79 / 39
$CH_2OH* + H* \rightleftharpoons CH_3OH*$					95 / 108
$CH_2O* + H* \rightleftharpoons CH_2OH*$					123 / 62
$CH_3* + OH* \rightleftharpoons CH_3OH*$					212 / 142

7.5 Model responses vs. experimental results at 484 K

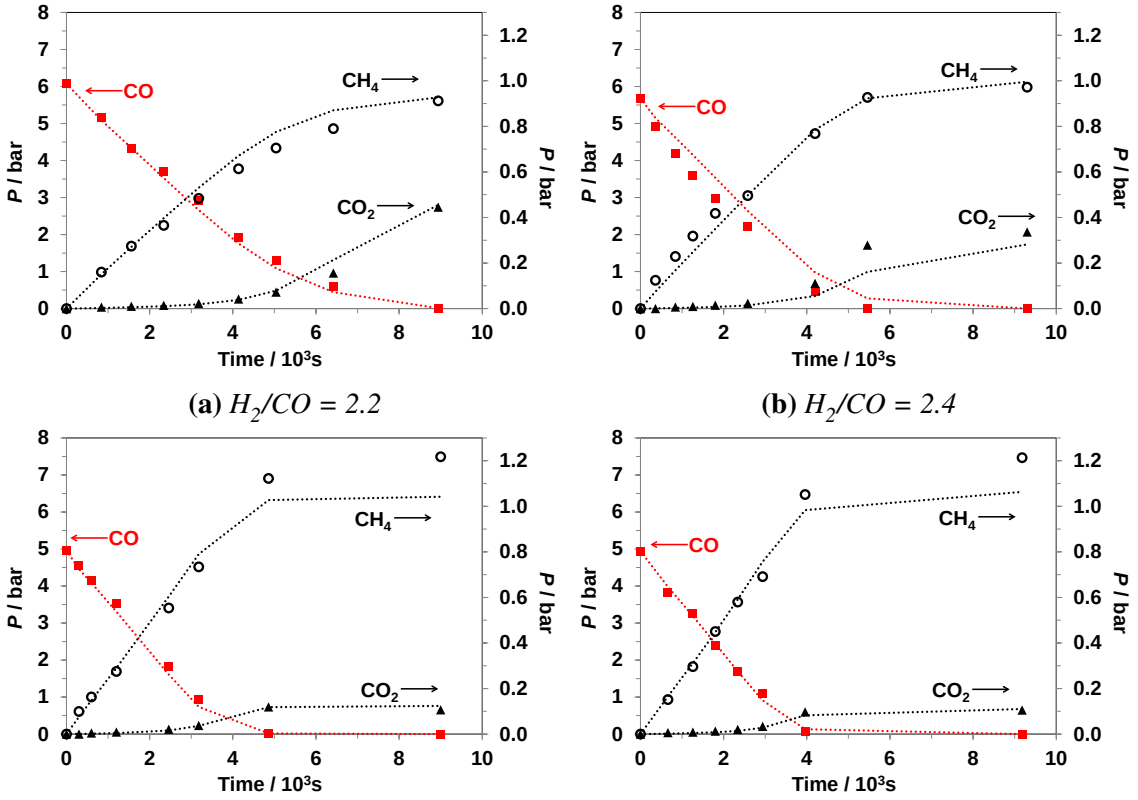

(a) $H_2/CO = 2.2$ **(b)** $H_2/CO = 2.4$

(c) $H_2/CO = 2.8$ **(d)** $H_2/CO = 2.9$

Figure S.4: *The partial pressures of C_1 species at 484 K and different H_2/CO ratios.*

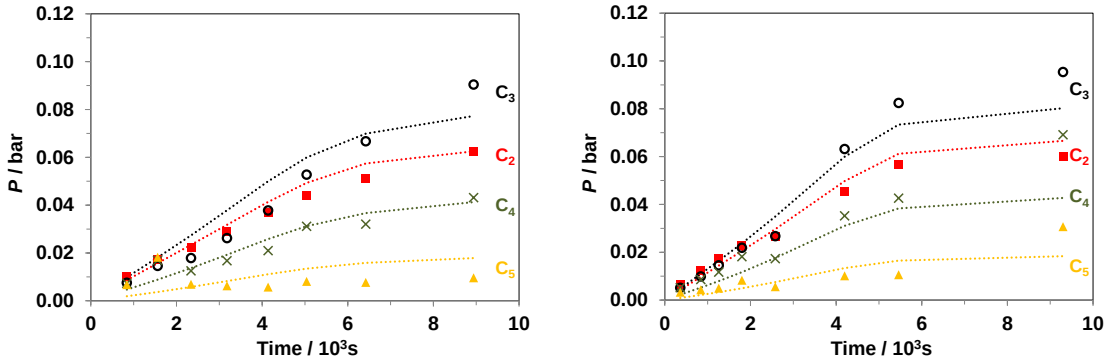

(a) $H_2/CO = 2.2$ **(b)** $H_2/CO = 2.4$

(c) $H_2/CO = 2.8$ **(d)** $H_2/CO = 2.9$

Figure S.5: *The partial pressures of paraffins at 484 K and different H_2/CO ratios.*

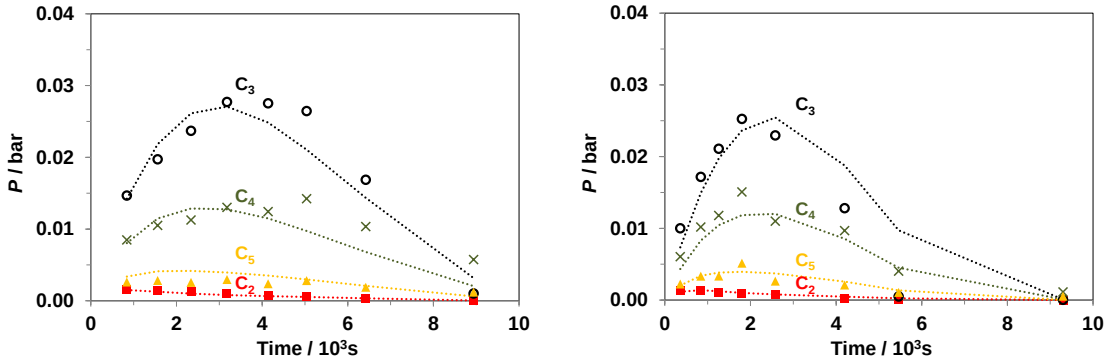

(a) $H_2/CO = 2.2$

(b) $H_2/CO = 2.4$

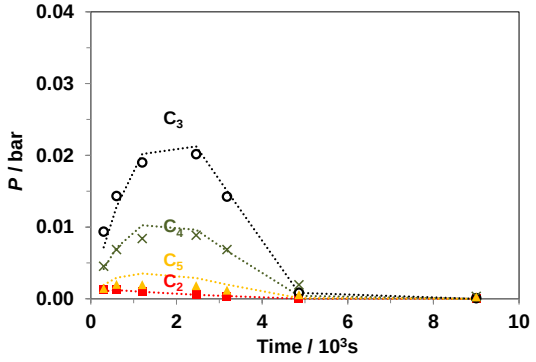

(c) $H_2/CO = 2.8$

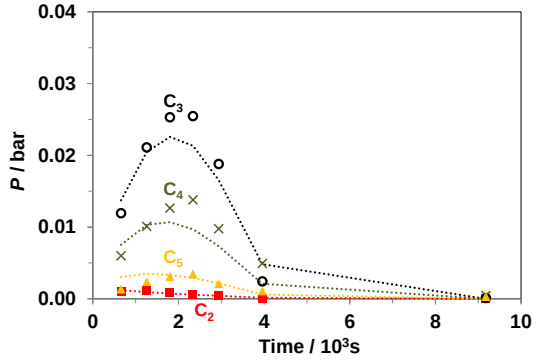

(d) $H_2/CO = 2.9$

Figure S.6: *The partial pressures of olefins at 484 K and different H_2/CO ratios.*

References

[1] G. L. Bezemer et al. “Cobalt Particle Size Effects in the Fischer-Tropsch Reaction Studied with Carbon Nanofiber Supported Catalysts”. In: *J. Am. Chem. Soc.* 128.12 (2006), pp. 3956–3964.

[2] Ø. Borg et al. “Fischer-Tropsch synthesis: Cobalt particle size and support effects on intrinsic activity and product distribution”. In: *J. Catal.* 259.2 (2008), pp. 161–164.

[3] J. P. den Breejen et al. “On the Origin of the Cobalt Particle Size Effects in Fischer-Tropsch Catalysis”. In: *J. Am. Chem. Soc.* 131.20 (2009), pp. 7197–7203.

[4] G. Brownbridge et al. “Automated IC engine model development with uncertainty propagation”. In: *SAE Paper No. 2011-01-0237* (2011).

[5] J. Cheng et al. “A First-Principles Study of Oxygenates on Co Surfaces in Fischer-Tropsch Synthesis”. In: *J. Phys. Chem. C* 112.25 (2008), pp. 9464–9473.

[6] J. Cheng et al. “A quantitative determination of reaction mechanisms from density functional theory calculations: Fischer-Tropsch synthesis on flat and stepped cobalt surfaces”. In: *J. Catal.* 254.2 (2008), pp. 285–295.

[7] B. H. Davis. “Fischer-Tropsch synthesis: current mechanism and futuristic needs”. In: *Fuel Process. Technol.* 71.1–3 (2001), pp. 157–166.

[8] M. E. Dry. “The Fischer-Tropsch process: 1950-2000”. In: *Catal. Today* 71.3–4 (2002), pp. 227–241.

[9] S. A. Goddard et al. “Kinetic simulation of heterogeneous catalytic processes: Ethane hydrogenolysis over supported group VIII metals”. In: *J. Catal.* 117.1 (1989), pp. 155–169.

[10] R. Hooke and T. A. Jeeves. ““Direct Search” Solution of Numerical and Statistical Problems”. In: *J. ACM* 8.2 (1961), pp. 212–229.

[11] E. Iglesia. “Design, synthesis and use of cobalt-based Fischer-Tropsch synthesis catalysts”. In: *Appl. Catal., A* 161 (1997), p. 59.

[12] O. R. Inderwildi, S. J. Jenkins, and D. A. King. “Fischer-Tropsch Mechanism Revisited: Alternative Pathways for the Production of Higher Hydrocarbons from Synthesis Gas”. In: *J. Phys. Chem. C* 112.5 (2008), pp. 1305–1307.

[13] S. Krishnamoorthy et al. “An Investigation of the Effects of Water on Rate and Selectivity for the Fischer-Tropsch Synthesis on Cobalt-Based Catalysts”. In: *J. Catal.* 211.2 (2002), pp. 422–433.

[14] A. J. Markvoort et al. “Kinetics of the Fischer-Tropsch Reaction”. In: *Angew. Chem. Int. Ed.* 51.36 (2012), pp. 9015–9019.

[15] D. Marquardt. “An Algorithm for Least-Squares Estimation of Nonlinear Parameters”. In: *J. Soc. Ind. Appl. Math.* 11.2 (1963), pp. 431–441.

[16] S. Mosbach et al. “Iterative improvement of Bayesian parameter estimates for an engine model by means of experimental design”. In: *Combust. Flame* 159.3 (2012), pp. 1303–1313.

[17] S. Mosbach et al. “Bayesian Error Propagation for a Kinetic Model of n-Propylbenzene Oxidation in a Shock Tube”. In: *Int. J. Chem. Kinet.* 46.7 (2014), pp. 389–404.

[18] J. Murray and D. King. “Climate policy: Oil’s tipping point has passed”. In: *Nature* 481.7382 (2012), pp. 433–435.

[19] M. Ojeda et al. “CO activation pathways and the mechanism of Fischer-Tropsch synthesis”. In: *J. Catal.* 272.2 (2010), pp. 287–297.

[20] M. Ojeda et al. “Kinetically Relevant Steps and H_2/D_2 Isotope Effects in Fischer-Tropsch Synthesis on Fe and Co Catalysts”. In: *J. Phys. Chem. C* 114.46 (2010), pp. 19761–19770.

[21] S. Shetty and R. A. van Santen. “CO dissociation on Ru and Co surfaces: The initial step in the Fischer-Tropsch synthesis”. In: *Catal. Today* 171.1 (2011), pp. 168–173.

[22] I. M. Sobol. “On the Systematic Search in a Hypercube”. In: *SIAM J. Numer. Anal.* 16.5 (1979), pp. 790–793.

[23] S. Storsæter, D. Chen, and A. Holmen. “Microkinetic modelling of the formation of C_1 and C_2 products in the Fischer-Tropsch synthesis over cobalt catalysts”. In: *Surf. Sci.* 600.10 (2006), pp. 2051–2063.

[24] S. Vada, B. Chen, and J. G. Goodwin. “Isotopic Transient Study of La Promotion of Co/Al_2O_3 for CO Hydrogenation”. In: *J. Catal.* 153.2 (1995), pp. 224–231.

[25] C. Visconti et al. “Detailed Kinetics of the Fischer-Tropsch Synthesis on Cobalt Catalysts Based on H-Assisted CO Activation”. In: *Top. Catal.* 54.13-15 (2011), pp. 786–800.